Real-Time Surface Analysis of Individual Airborne Environmental Particles

ARTICLE *in* ENVIRONMENTAL SCIENCE AND TECHNOLOGY · OCTOBER 1999

Impact Factor: 5.33 · DOI: 10.1021/es9905849

4 AUTHORS, INCLUDING:

Peter T A Reilly
Washington State University
62 PUBLICATIONS **1,122** CITATIONS

SEE PROFILE

Environ. Sci. Technol. **1999**, *33,* 3993−4001

Real-Time Surface Analysis of Individual Airborne Environmental Particles

ALEXANDRU C. LAZAR, PETER T. A. REILLY,* WILLIAM B. WHITTEN, AND J. MICHAEL RAMSEY

Oak Ridge National Laboratory, P.O. Box 2008, M/S 6142, Oak Ridge, Tennessee 37831-6142

Typically, in real-time aerosol mass spectrometry (RTAMS), individual airborne particles are ablated and ionized with a single focused laser pulse. This technique yields information that permits bulk characterization of the particle, but information about the particle's surface is often masked or diluted by the particle bulk. Here we show that it is possible to probe the surface composition of individual airborne particles by separating the desorption and ionization steps using a two-laser real-time aerosol mass spectrometry technique (L2RTAMS). First, a weak excimer laser pulse was used to desorb the semivolatile components of the particle surface when the particle was in the center of the ion trap. After a short delay, another excimer laser pulse was used to ionize the semivolatile surface components in the gas phase and subsequently mass analyzed. The results from the one- and two-laser techniques were compared and found to be complementary. The L2RTAMS technique was found very sensitive to polycyclic aromatic hydrocarbons (PAHs). PAHs, of the type emitted from diesel engines, were found on particle surfaces of National Institute of Standards and Technology (NIST) standard reference materials (SRMs) from Indiana Harbor Canal (1645) and urban particulate matter (1648). PAH partitioning on the environmental particles is discussed.

Introduction

In the atmosphere, airborne particles are dynamic. Their compositions change with time and environment by reaction, adsorption/desorption, condensation, and aggregation. All of these processes occur at the particle surface. The dynamics of these processes are not well understood and are difficult to characterize due to the diverse and changing nature of the particles that make up the ambient aerosol.

Over the past decade, great progress has been made in understanding the diverse nature of ambient aerosols. Several research groups have reported real-time analysis of individual airborne particles using mass spectrometry (*1*−*8*). These groups analyze individual ablated and ionized particles using a time-of-flight mass spectrometer (TOF MS) in real-time and have had great success in characterizing inorganically based particles. However, success at analyzing organic material has been limited because high yields of fragment ions from organic species make identification of components in a mixture untenable. Using an ion trap as a mass analyzer, our group has shown that tandem mass spectrometry can be used to identify organic ions from individual particles made up of complex mixtures (*9*−*11*).

At first glance, it seemed that the ability to size and measure the mass spectrum of individual particles in an ambient aerosol would yield all the information required to fully characterize any aerosol. Unfortunately, laser ablation mass spectra do not yield comprehensive information. Careful analysis of standard reference materials (SRMs) from the Nation Institute of Standards and Technology (NIST) have shown that charge-transfer-induced matrix effects can cause dramatic changes in sensitivities ranging from parts per million to completely insensitive, depending upon the matrix characteristics (*12*). Therefore, assigning the concentration of a given species in an environmental aerosol on an individual particle basis where the matrix is substantially changing from particle to particle is not credible.

These charge-transfer-induced matrix effects occur in the ablation plume (*12*). They can be minimized by separating the ablation and ionization events. Evidence of this effect in real-time aerosol mass spectrometry was first reported in the literature by Morrical and co-workers (*13*) where they used two lasers to separate the ablation and ionization events. However, their assertion that the difference between the results of two-laser and one-laser experiments was due to the fragility of the organic species suggesting that the two-laser was a "soft" desorption/ionization technique was only correct for the pure dihydroxybenzoic acid particles. In the case of their "real world" samples that are essentially complex mixtures, the primary difference in the results for one or two lasers was due to charge-transfer-induced matrix effects. The presence of one-laser ionization matrix effects has been well established in the literature by the groups using two-laser desorption/ionization mass spectrometry (L2MS) to measure the composition of particles suspended on various substrates (*14*−*18*).

This paper presents a variation on the two-laser real-time aerosol mass spectrometry experiment. Here we have reduced the power of the desorption laser so that the semivolatile species are desorbed from the particle surface without substantially ablating the bulk of the particle. This permits, for the first time, the probing of the chemical composition of species loosely bound to individual particle surfaces in real-time.

In this paper, we present a study of PAHs adsorbed on individual environmental particles in real-time. The samples studied were standard reference materials (SRMs 4353, 1648, and 1645) from the National Institute of Standards and Technology (NIST). Since the samples were collected years in the past, volatile surface components have long ago evaporated. Only the semivolatile components were left, and it was assumed that the partitioning of the semivolatile components among the particles was equilibrated so that all of the particles in the sample have had sufficient time to interact so that transfer of the surface species between the particles has reached equilibrium.

In the future, this technique will permit the study of particle−gas phase, particle−particle, and particle−surface interactions of systems that have not been equilibrated. This will provide information on the role of the particle surface in mass transport and as a reaction medium. The information this technique provides will greatly enhance our understanding of the role that particles play in the chemistry of the atmosphere as well as the role that they play in affecting our health.

* Corresponding author telephone: (423)574-4919; fax: (423)574-8363; e-mail: ReillyPT@ORNL.GOV.

10.1021/es9905849 CCC: $18.00
Published on Web 10/12/1999

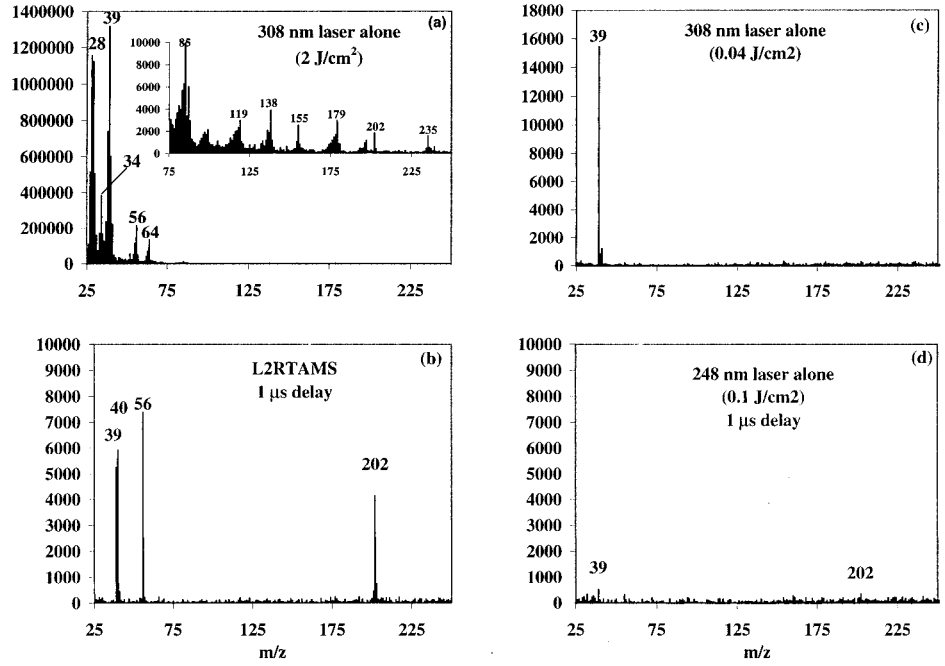

FIGURE 1. (a) One-laser particle mass spectrum of Rocky Flats soil (NIST SRM 4353) spiked with 200 μg/g of pyrene averaged from 272 individual particle mass spectra. Only the 308-nm excimer laser was used at a fluence of 2 J/cm^2. (b) Two-laser particle mass spectrum of the same sample averaged from 154 individual particle mass spectra. The 308-nm desorption laser fluence was 0.04 J/cm^2. The 248-nm ionization laser fluence was 0.10 J/cm^2. There was a 1-μs delay between the desorption and ionization lasers. The focal points of the counterpropagating desorption and ionization lasers were spatially overlapped. (c) Particle mass spectrum of the same sample averaged from 159 individual particles using only the 308-nm desorption laser (0.04 J/cm^2). (d) Particle mass spectrum of the same sample averaged from 151 individual particles using only the 248-nm ionization laser (0.10 J/cm^2) delayed by 1 μs.

Experimental Section

The experimental apparatus has been described in detail elsewhere (*19*−*21*). To summarize the experiment, soil aerosols were generated by passing dry air through a container holding the sample. A portion of the sample was aerosolized by continuous agitation with a magnetic stirrer. The particle-laden air was then introduced to the inlet of the mass spectrometer. The inlet was differentially pumped and consisted of an inverted nozzle and two skimmers. This setup created a well-collimated particle beam inside the vacuum chamber that passed through the center of the ion trap. Upon entering the main chamber, the particles passed through two focused Ar^+ ion lasers and scattered light. The scattered light was collected by fiber optics at each detection point and detected at two separate photomultiplier tubes (PMTs). The signals from the PMTs were converted to TTL levels and then used to record the particle time-of-flight between the detection points and fire the lasers when the particle arrived at the center of the ion trap regardless of size or velocity.

When the particles reached the center of the ion trap, a focused 308-nm XeCl excimer laser was fired to desorb the surface species of the individual particles. After a short 0.3−1-μs delay, a focused 248 KrF excimer laser was fired to ionize the desorbed neutral species. The focal points of the counterpropagating lasers were spatially overlapped in the center of the ion trap. The typical laser fluence of the 308-nm laser during the single-laser experiments was approximately 2 J/cm^2. During the two-laser experiments, the fluence of the desorption and ionization lasers was reduced to 0.04 and 0.1 J/cm^2, respectively, using neutral density filters. At these intensities, only a limited number of the laser shots from either laser alone produced a measurable ion signal; however, when they were combined, the ion signals were much more intense and frequent.

The system was first tested using Rocky Flats soil (NIST SRM 4353) because it showed no evidence of PAHs in the one-laser experiments even on an individual particle basis. This sample (~1 g) was then spiked to 200 mg/g concentration by adding and evaporating a 100 μg/mL pyrene solution. The spiking solution was made by first dissolving the pyrene in 1 mL of benzene and diluting the solution to 100 mL with acetone. The system was then tested using Indiana Harbor Canal sediment (NIST SRM 1645) and urban particulate matter from St. Louis, MO, air (NIST SRM 1648) (*12*). The measured size distributions of the SRMs were all found similar. Many of them can be found in ref *12*.

Results and Discussion

The capabilities of the L2RTAMS technique for surface analysis were first assessed using Rocky Flats soil (NIST SRM 4353) spiked with pyrene. Figure 1a shows the average of 272 individual soil particle mass spectra. Each mass spectrum was taken with a single laser pulse from the 308-nm excimer laser (2 J/cm^2) used to ablate and ionize each individual particle. A 200 μg/g pyrene/soil sample readily yielded a detectable signal (m/z 202) in the one-laser experiment (see inset in Figure 1a). This concentration yielded approximately a 2-Å thick layer of pyrene on the particle surfaces (i.e., on the order of a monolayer). All of the mass lines in the one-laser experiment except the single pyrene line at m/z 202 were the result of the particle matrix. Given the singularity of the pyrene line (i.e., the lack of any evidence of hydrogen loss or gain from pyrene), there was little evidence of any laser-induced fragmentation even under the high-intensity conditions of the one-laser experiment. Since pure pyrene particles readily undergo pyrolysis-induced fragmentation at this laser fluence (*22*), the particle matrix must be acting as a large energy sink to keep the pyrene from fragmenting.

Figure 1b shows the results of the L2RTAMS technique on the same pyrene/Rocky Flats soil sample as in Figure 1a. It is an average of 154 individual soil particle spectra. The ionization laser was fired after a 1-μs delay following the desorption laser. Comparison of panels a and b in Figure 1 showed a dramatic increase in the signal-to-noise ratio of

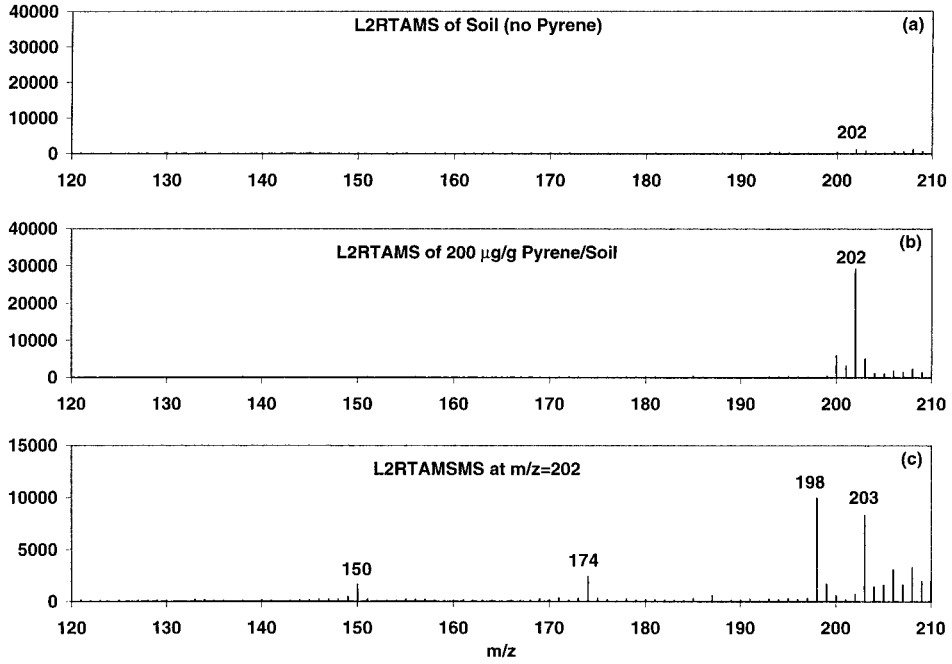

FIGURE 2. (a) Isolation spectrum of *m/z* 202 from the two-laser desorption/ionization of Rocky Flats soil (NIST SRM 4353) without added pyrene averaged from 88 individual particle mass spectra. The 308-nm desorption laser fluence was 0.04 J/cm^2. The 248-nm ionization laser fluence was 0.10 J/cm^2. There was a 1-μs delay between the desorption and ionization lasers. (b) Isolation spectrum of *m/z* 202 from the two-laser desorption/ionization of Rocky Flats soil (NIST SRM 4353) with added pyrene averaged from 175 individual particle mass spectra under identical conditions. (c) Product ion spectrum of *m/z* 202 after CAD averaged from 157 individual particles from the same pyrene spiked Rocky Flats sample.

the pyrene mass line for the two-laser technique. Also evident in the spectrum were mass lines at m/z 39, 40, and 56 representing K^+, Ca^+, and CaO^+, respectively. The same sample was measured using only the desorption laser (308 nm) and then only the ionization laser (248 nm) delayed by 1 μs. The results of these experiments are in Figure 1, panels c and d, respectively. Figure 1c is an average of 159 individual particle spectra and shows only a strong potassium ion line at m/z 39. Figure 1d is an average of 151 individual particle spectra and reveals no significant production of ions above the noise level. Comparison of Figure 1, panels b and c, shows that the potassium ions (m/z 39) were created using only the desorption laser in what is most likely a one-photon process that involves dissociation of potassium salts that were part of the particle surface. Ca and CaO were desorbed as neutral species and subsequently ionized by the second laser.

Figure 2 demonstrates the ability of the ion trap incorporating the two-laser RTAMS technique to positively identify organic species at monolayer coverages or lower using tandem mass spectrometry. Figure 2a shows the averaged L2RTAMS spectrum of the Rocky Flats soil without the addition of pyrene. (There are 88 individual particle spectra in the average.) The small amount of signal at m/z 202 in this spectrum is probably due to a small background of combustion-related material adsorbed on the particle surfaces. However, this concentration of material is negligible in comparison to the amount of pyrene on the spiked soil sample seen in Figure 2b. This spectrum is an average of 175 individual particle spectra. It shows an analyte signal that is 25 times greater than the background. Therefore, the background signal did not significantly contribute to the analyte signal in the spiked sample. Tandem mass spectrometry (MS/MS) was subsequently performed on the pyrene desorbed and then ionized from the spiked sample surfaces. The pyrene molecular ion was isolated in the ion trap and then excited at its secular frequency in the trap. This excitation caused collision-activated dissociation (CAD) of the m/z 202 ion in the He bath gas (~1 mTorr). The averaged product ion spectrum of m/z 202 from 157 individual particles is shown in Figure 2c. It shows characteristic loss of hydrogen from the parent ion down to m/z 198. The degree of hydrogen loss is dependent upon the CAD conditions. More or less hydrogen loss can result by changing the tickle voltage and duration. The product ion spectrum also reveals characteristic loss of C_2H_4 and C_4H_4 to produce daughter ions at m/z 174 and 150, respectively. This spectrum is essentially congruent with the results observed by Nourse and co-workers (*23*). It shows that the pyrene is largely unfragmented by the desorption/ionization process of the two-laser technique.

In a previous publication (*12*), we demonstrated that PAHs were detectable in the average mass spectrum using the one-laser RTAMS technique on Indiana Harbor Canal sediment (NIST SRM 1645) if one adjusted the trapping conditions to augment the sensitivity toward the higher masses. Consequently, under typical trapping conditions used in the present study for the one-laser experiments, the presence of the PAHs in the averaged mass spectrum was not readily apparent (see Figure 3a). However, when the L2RTAMS technique was used, the presence of the PAHs on the surfaces of the individual particles became apparent. The data in Figure 3 were taken on the same day under identical sample and trapping conditions. Only the nature of the desorption/ionization process was changed. These two averaged spectra demonstrate the magnitude of the matrix effect in the one-laser experiment. The absorption cross sections of the PAHs do not change by more than an order of magnitude from 248 to 308 nm. For example, the log ϵ of chrysene ($C_{18}H_{12}$ m/z 228) is 4.3 at 248 nm and 4.0 at 308 nm (*24*). Accordingly, the PAH ion signal intensity from our one-laser experiment should have been an order of magnitude greater than the signal from the two-laser experiment, assuming that the ionization of the PAHs did not saturate. Instead, we saw the reverse. The signal from the two-laser experiment was an order of magnitude more intense than the signal from the one-laser experiment. In our previous publication (*12*), we

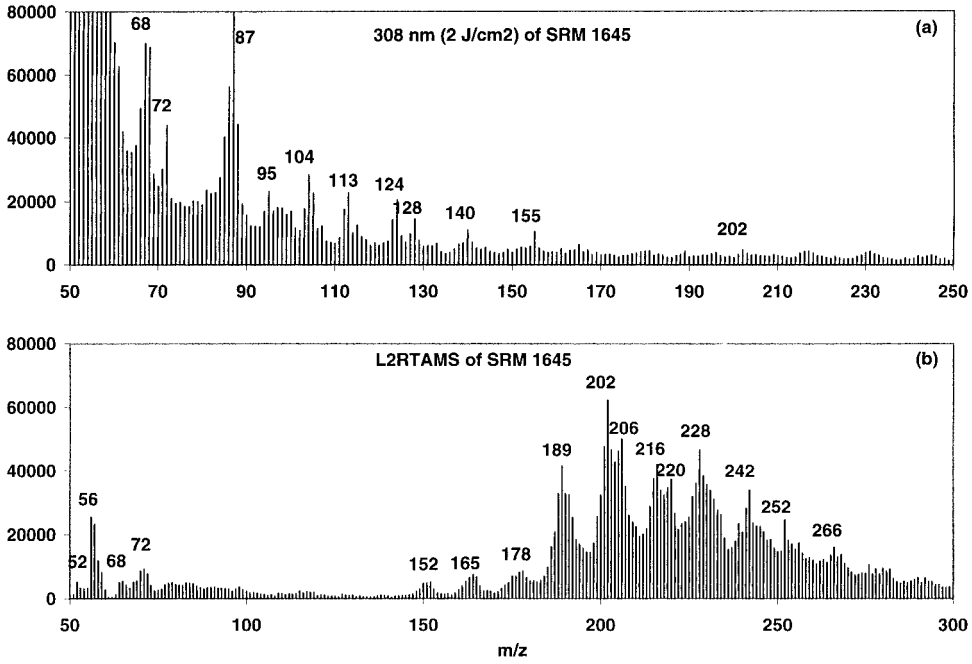

FIGURE 3. Comparison of the one- and two-laser RTAMS techniques. (a) One-laser particle mass spectrum of Indiana Harbor Canal sediment (NIST SRM 1645) averaged from 225 individual particle mass spectra. Only the 308-nm excimer laser was used at a fluence of 2 J/cm^2. (b) Two-laser particle mass spectrum of the same sample averaged from 134 individual particle mass spectra. The 308-nm desorption laser fluence was 0.04 J/cm^2. The 248-nm ionization laser fluence was 0.10 J/cm^2. There was a 1-μs delay between the desorption and ionization lasers. The focal points of the counterpropagating desorption and ionization lasers were spatially overlapped.

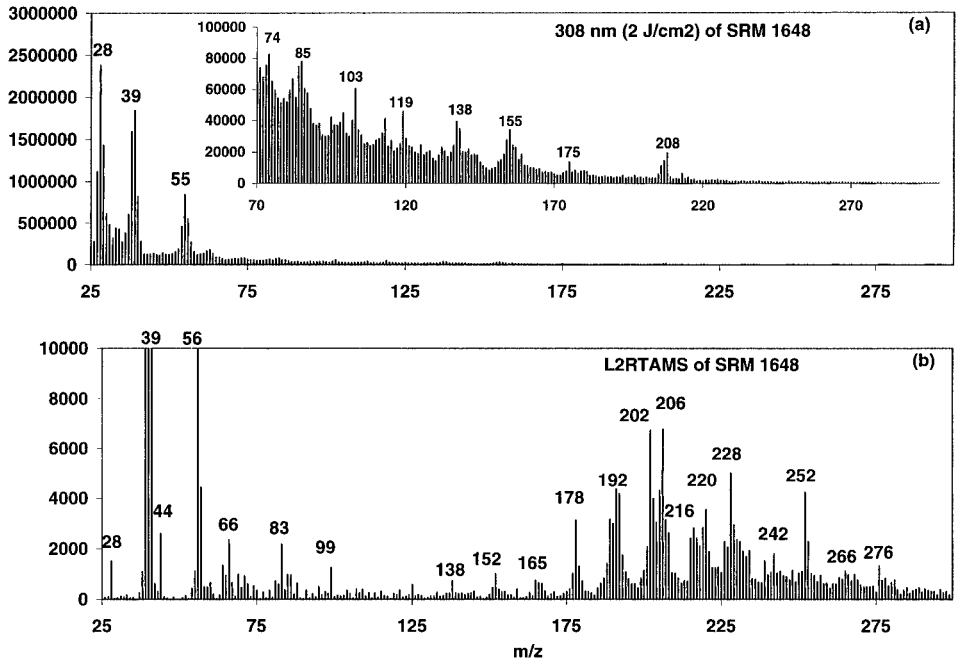

FIGURE 4. Comparison of the one- and two-laser RTAMS techniques on urban particulate matter from St. Louis air (NIST SRM 1645). (a) One-laser particle mass spectrum averaged from 335 individual particle mass spectra. Only the 308-nm excimer laser was used at a fluence of 2 J/cm^2. (b) Two-laser particle mass spectrum averaged from 183 individual particle mass spectra. The 308-nm desorption laser fluence was 0.04 J/cm^2. The 248-nm ionization laser fluence was 0.10 J/cm^2. There was a 1-μs delay between the desorption and ionization lasers. The focal points of the counterpropagating desorption and ionization lasers were spatially overlapped.

demonstrated that this matrix effect is the result of charge transfer that occurs during the ablation step where the ions undergo many collisions with the much more numerous neutral species. This type of matrix effect is not present in the two-laser experiment. Consequently, it is reasonable to expect this technique to provide accurate qualitative as well as quantitative analysis of the semivolatile species bound to the surfaces of individual airborne particles.

In that same publication (*12*), we were also surprised when we observed no evidence of PAHs in the averaged particle mass spectrum from urban particulate matter collected in St. Louis, MO (NIST SRM 1648). We had expected to see PAHs emitted from motor vehicles, especially diesel-fueled trucks, yet none were seen in the average spectrum. Moreover, even when the hundreds of individual particle mass spectra from SRM 1648 were viewed, there was no sign of what could

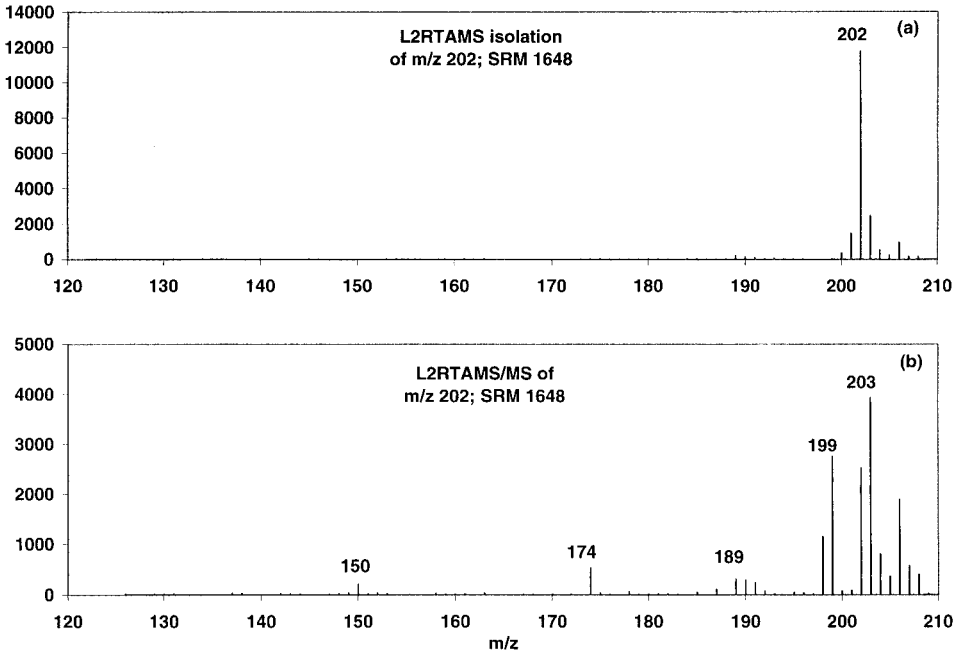

FIGURE 5. (a) Isolation spectrum of *m/z* 202 from the two-laser desorption/ionization of on urban particulate matter from St. Louis air (NIST SRM 1645) averaged from 350 individual particle mass spectra. The 308-nm desorption laser fluence was 0.04 J/cm^2. The 248-nm ionization laser fluence was 0.10 J/cm^2. There was a 1-μs delay between the desorption and ionization lasers. (b) Product ion spectrum of *m/z* 202 after CAD averaged from 165 individual particles from the same sample.

be construed as PAH-containing soot particles (*25*), even though 30−50% of the fine particle mass in urban aerosols comes from fine carbon particles that are primarily derived from combustion sources (*26*).

Consequently, we thought that SRM 1648 would be a good candidate for surface studies since the PAHs from the combustion aerosols are known to bind strongly to geosorbents (*27*). We expected to find evidence of the PAHs on wind-blown soil particles in the sample. The results of the one-laser experiment are shown in Figure 4a. This spectrum is the average of 335 individual particle spectra. Once again, no sign of PAHs was observed in the average spectrum from the one-laser RTAMS experiment. However, when we applied the L2RTAMS technique to the sample (see Figure 4b), the presence of the PAHs on the particle surfaces became patently clear.

In the NIST SRMs in this publication, we observed PAH mass distribution patterns that were typical of combustion-generated particles from pine (*25*) and acetylene flames (*28*) at *m*/*z* 152, 166, 178, 190, 202, 216, 228, 242, 252, 266, 276, etc. However, superimposed on these distributions were peaks at *m*/*z* 206 and 220 in both samples. To demonstrate our ability to perform tandem mass spectrometric analysis on species adsorbed on the surfaces of individual real-world environmental particles, we performed the L2RTAMS/MS experiment at *m*/*z* 202 on the particles in the urban particulate matter sample (NIST SRM 1648). The results of this experiment can be seen in Figure 5. Figure 5a demonstrates our ability to isolate the *m*/*z* 202 ions from the rest of the ions generated in the L2RTAMS experiment; it represents the average isolation spectrum from 350 individual particles of SRM 1648. Figure 5b shows the averaged product ion spectrum from CAD of *m*/*z* 202 ions produced using the L2RTAMS technique on 165 individual particles from the SRM 1648 sample. These results compared well with the results seen from the pyrene-spiked Rocky Flats soil sample (NIST SRM 4353), suggesting that the primary component of the 202 ions be derived from pyrene-like PAHs. However, there was also a local product ion distribution that peaks at *m*/*z* 189. Similar results were found when we performed

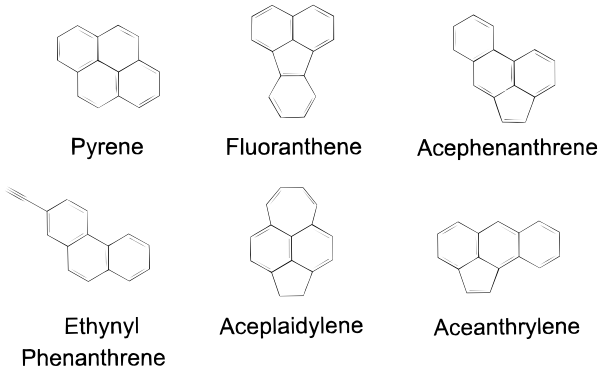

FIGURE 6. Some possible *m/z* 202 isomers. The CAD product ion spectra of these isomers should be very similar because PAHs rearrange before they fragment.

tandem mass spectrometric analysis of the 202 ions generated from RTAMS of flame-generated acetylene soot (*22*). The nature of the *m*/*z* 202 component(s) that yielded the *m*/*z* 189 distribution is unclear because there is a variety of $C_{16}H_{10}$ isomers, some of which are shown in Figure 6. These isomers are not readily distinguished by the tandem mass spectrometric technique because they rearrange before they fragment (*23*). However, one or more isomers could conceivably yield the *m*/*z* 189 fragment preferentially. More work with pure isomers is needed to resolve this issue. Identifying PAH isomers using mass spectrometry is an ongoing problem.

In our study of diesel-engine-generated emissions (*25*), we noted the detection of hydrogenated PAHs (HPAHs) whose presence was a consequence of hydrogenation of the diesel fuel at the refinery. HPAHs are not, in general, stable in the environment and should revert to PAHs under atmospheric conditions. However, there are probably forms of HPAHs that are stable even in the particle phase where the surface area to volume ratio is extremely high. We therefore suspected that the distributions at *m*/*z* 206 and 220 might be due to hydrogenated PAHs as opposed to alkylated phenanthrenes as suggested in the literature (*29*). Consequently, we ran the L2RTAMS/MS experiment to determine the structure of the

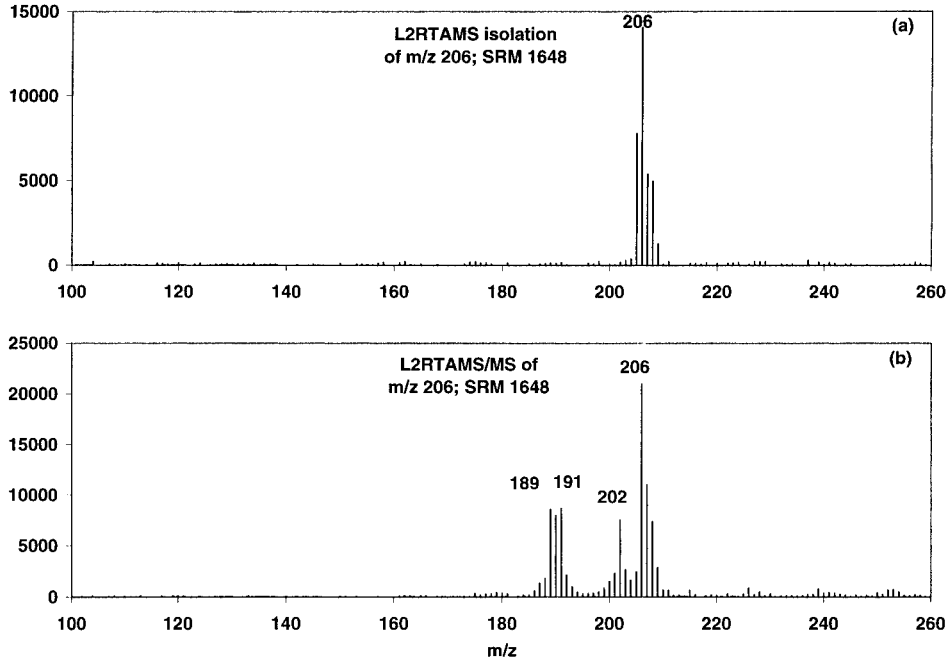

FIGURE 7. (a) Isolation spectrum of *m/z* 206 from the two-laser desorption/ionization of on urban particulate matter from St. Louis air (NIST SRM 1645) averaged from 350 individual particle mass spectra. The 308-nm desorption laser fluence was 0.04 J/cm². The 248-nm ionization laser fluence was 0.10 J/cm². There was a 1-μs delay between the desorption and ionization lasers. (b) Product ion spectrum of *m/z* 206 after CAD averaged from 165 individual particles from the same sample.

m/*z* 206 ions. The results are shown in Figure 7. Panel a shows the averaged isolation from 67 individual particles from the SRM 1648 sample. Panel b reveals the averaged product ions spectrum from 68 individual particles from the same sample. This spectrum looks remarkably similar to the product ion spectrum of *m*/*z* 206 revealed in our diesel engine emissions study (*25*). In that study, we took the presence of the peak at *m*/*z* 202 as confirmation of the presence of HPAHs; we do the same here. However, we cannot wholly exclude the presence of the alkylated phenanthrenes such as 2,3-dimethylphenanthrene or 2-ethylphenanthrene based on our MS/MS results alone because their major fragments are found at *m*/*z* 189 and191 in the electron impact spectra (*24*). Therefore, alkylated phenanthrenes could be a major component of the ions of *m*/*z* 206 on that basis. However, if this is true, then one would expect to find these same alkylated PAHs in similar abundance in combustion-generated particles where the fuel has not been hydrogenated. Since significant amounts of *m*/*z* 206 and 220 were not observed in the pine smoke (*25*) and acetylene soot (*28*), the presence of alkylated PAHs is probably not significant in these samples.

If this assumption is correct, the presence of *m*/*z* 206 and 220 can be used as markers for particles generated from the combustion of hydrogenated fuels in environmental aerosols. If one remembers that most HPAHs revert to their normal PAH form upon interaction with the atmosphere, then one quickly comes to the realization that the majority of the PAHs that are observed on the surfaces of the particles in these environmental samples (NIST SRM 1645 and 1648) are probably coming from sources that use hydrogenated fuels, primarily diesel engines.

The fluences of the desorption and ionization lasers were carefully chosen. The intensity of the desorption laser was chosen by experiment to minimize the signal generated by this laser alone while maximizing the signal generated by the two-laser experiment (see Figure 1c). The intensity of the ionization laser was set to yield no significant signal from the particle by itself. However, this intensity is enough to saturate most resonant (1 + 1) multiphoton ionization processes. In other words, the majority of the gas-phase species that have a significant adsorption cross section at 248 nm should be completely ionized. Therefore, most of the relative total ion count fluctuations that we see in our L2RTAMS spectra should be due to fluctuations in the intensity with which the desorption laser hits the particle and in the surface composition of the particles. These effects can be observed by judiciously sorting and averaging the data.

There is a broad range of desorption laser intensities that the particles may experience due to shot-to-shot fluctuations in the total pulse energy, hot spots in the focal point because the particle is much smaller than the focused laser spot, and timing jitter in the electronics that fires the lasers. Changes in the average particle spectrum that are the result of fluctuations in the intensity with which the desorption laser interacts with the particle can be observed by sorting the particle mass spectra as a function of relative total ion count (RIC), binning and averaging if the number of particles measured is large enough such that compositional fluctuations are averaged out. The results of this type of analysis for the urban particulate matter sample (NIST SRM 1648) can be seen in Figure 8. Here we have sorted 523 individual particle spectra as a function of relative total ion intensity (RIC) and binned them, arbitrarily setting the range of each to the following: $0 < \text{RIC} < 20000$, $20000 < \text{RIC} < 100000$, $100000 < \text{RIC} < 500000$, and $500000 < \text{RIC}$. The spectra in each bin were averaged. The averaged results of the 340 spectra in the $0 < \text{RIC} < 20000$ bin showed no coherent signal above the noise level (*30*). Therefore, these spectra were considered misses and were not shown. The averages of the bins are shown as a function of decreasing ion intensity in panels a−c, respectively, in Figure 8. The intensity of the potassium ion is a direct result of the desorption laser (see Figure 1). This ion's intensity is approximately 500 000 in panel a, 100 000 in panel b, and 5000 in panel c. The intensity of the *m*/*z* 206 ion is approximately15 000 in panel a, 6000 in panel b, and 1900 in panel c. In panel a, the presence of the ions at *m*/*z* 28, 44, 66, 83, 99, and 138 are indications that some of the particle surfaces in the ensemble are beginning to be ablated under these conditions. These results show

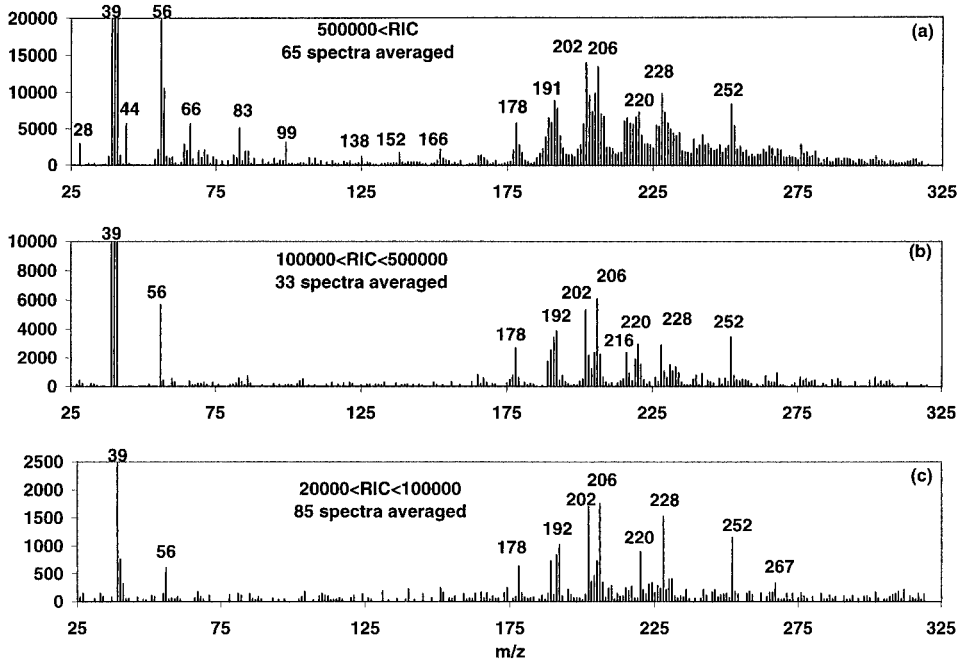

FIGURE 8. Urban particulate matter L2RTAMS spectra sorted as a function of total relative ion count (RIC). The spectra were sorted into four bins whose ranges were arbitrarily set to the following: 500000 < RIC, 100000 < RIC < 500000, 20000 < RIC < 100000, and 0 < RIC < 20000. The averages of these bins are shown in panels a−c, respectively. The average from the 0 < RIC < 20000 bin is not shown because there was no coherent signal above the noise level in the average.

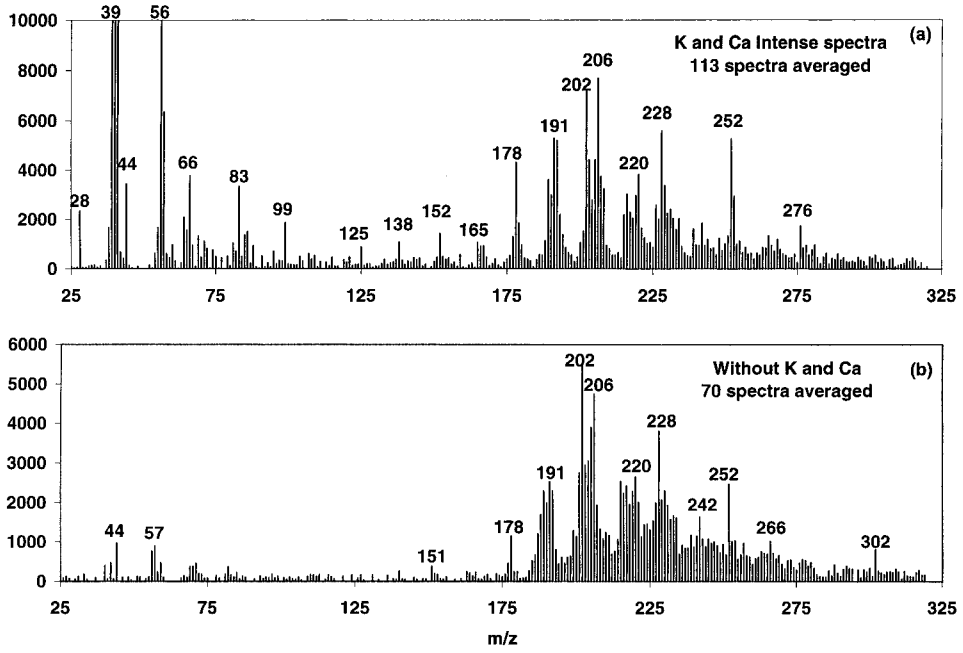

FIGURE 9. Urban particulate matter L2RTAMS spectra sorted as a function of potassium and calcium ion content. (a) The average of 113 potassium and calcium intense L2RTAMS individual particle spectra. (b) The average of the (70) leftover spectra without significant potassium and calcium ion intensity.

that the change in the RIC is an indication of the change in the strength of the desorption laser interaction.

It was understood that the particle substrates in these environmental samples were widely varying. For this reason, we attempted to sort the spectra as a function of surface composition. The most logical place to begin was to sort the spectra as a function of potassium and calcium content. The 113 spectra with intensity at m/z 39 and 40 were placed in one bin, and the 70 leftover spectra without were placed in another. The averages of these bins are shown in Figure 9, panels a and b, respectively. Comparison of these averaged spectra in this figure show a difference in the PAH distributions. Since the overall intensities of the PAH distributions are comparable, it may be assumed that the overall desorption laser interactions are also comparable. Consequently, the PAH distribution difference is probably not the result of pyrolysis induced by the desorption laser. Given the number of spectra in the averages, one would assume that shot-to-shot variations that result when identical particles are measured would average out. Consequently, the difference in the PAH distributions in these averages is most likely the result of partitioning of the PAHs that results from differences in the averaged substrate surface composition. More work is needed to explore PAH partitioning.

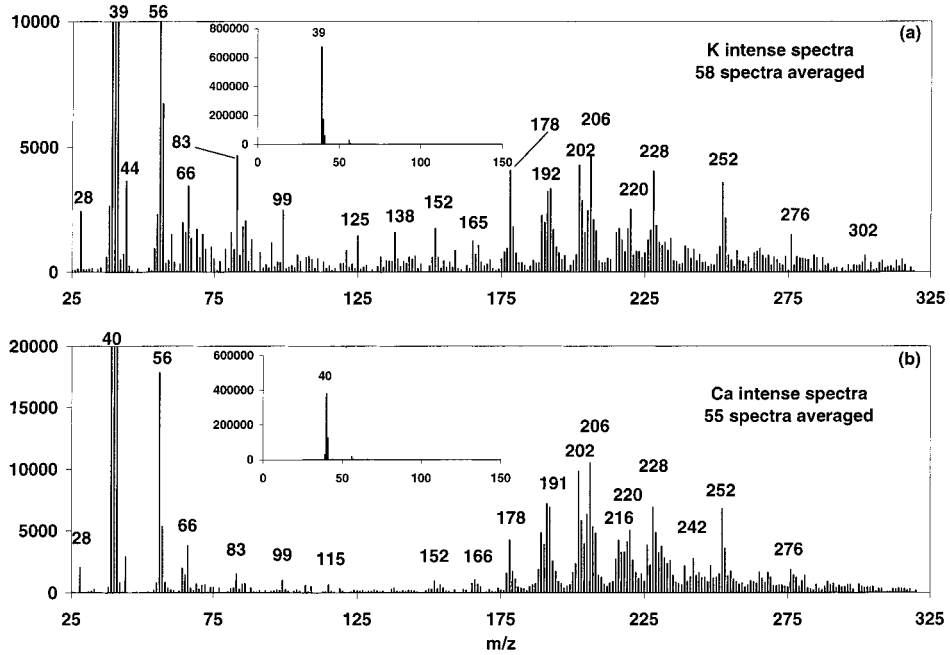

FIGURE 10. Urban particulate matter L2RTAMS spectra sorted as a function of potassium and calcium ion content. (a) The average from 58 potassium intense individual L2RTAMS particle spectra. The inset shows the averaged spectrum at full scale. (b) The average from 55 calcium intense individual L2RTAMS particle spectra. The inset shows the averaged spectrum at full scale.

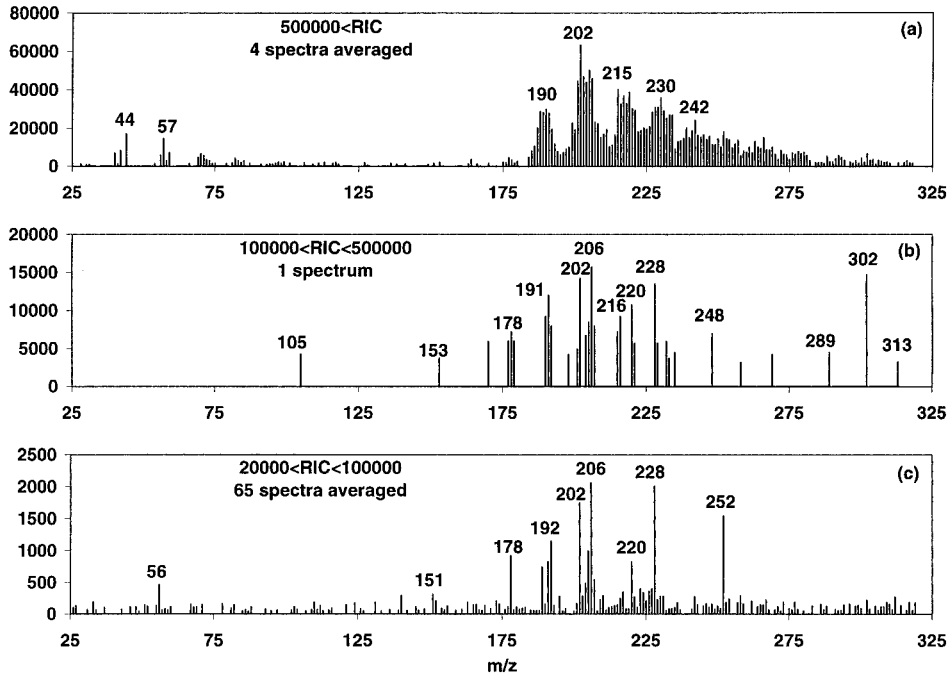

FIGURE 11. Urban particulate matter L2RTAMS spectra without significant potassium and calcium ion intensity sorted as a function of total relative ion count (RIC). The spectra were sorted into four bins whose ranges were arbitrarily set to the following: 500000 < RIC, 100000 < RIC < 500000, 20000 < RIC < 100000, and 0 < RIC < 20000. The averages of these bins are shown in panels a–c, respectively. The average from the 0 < RIC < 20000 bin is not shown because there was no coherent signal above the noise level in the average. Only four spectra were averaged in the 500000 < RIC bin and one in the 100000 < RIC < 500000 bin. The remaining 65 spectra were in the 20000 < RIC < 100000 bin.

Since potassium primarily desorbs from the surface as an ion, it is reasonable to assume that it exists on the particle surface as a salt. However, calcium desorbs primarily as a neutral. This suggests that the surfaces that contain calcium without much potassium are not as ionic. It seemed logical to pursue this concept of PAH partitioning as a function of surface composition further by sorting the K and Ca intense spectra as a function of m/z 39 intensity. The results of the averages from this sort are shown in Figure 10. Panel a reveals the PAH distribution averaged from 58 individual particle spectra whose surfaces should be fairly ionic due to the large potassium mass line intensity (see the inset in Figure 10 a). Panel b reveals the PAH distribution averaged from 55 individual particle spectra whose surfaces should be less ionic yet consistent due to the large calcium mass line intensity (see the inset in Figure 10 b). Comparison of the averaged spectra in Figure 10 reveals very similar overall PAH distributions. However, the overall relative intensities of the

PAH distributions differ by approximately a factor of 2. This demonstrates that PAHs preferentially adsorb on less ionic surfaces.

In Figure 9b, we observed that a narrower PAH distribution arose from particle surfaces that did not co-desorb potassium and calcium. These particle spectra were further sorted as a function of RIC into three bins with the same ranges as described previously. Of these 70 particle spectra, four were sorted into the 500000 < RIC bin, one into the 100000 < RIC < 500000 bin, and the remaining 65 into the 20000 < RIC < 100000 bin. The averages of the spectra in these bins are shown in Figure 11, panels a−c, respectively. After perusing these averages, it is immediately apparent that the majority of the particles that do not co-desorb potassium and calcium yield sharp local PAH distributions. Only the four spectra with the highest RIC values show broad local PAH distributions. Since these four spectra show such intense PAH distributions relative to the other 66 spectra that also do not co-desorb potassium and calcium, it is reasonable to suspect that these spectra are from combustion soot particles while the rest of the spectra come from particles that have small amounts of combustion soot PAHs partitioned on their surfaces, as suggested by the lack of PAH hydrogen exchange.

After carefully examining all of the data, we realized that the majority of the particles that yield enough ions to be considered "hits" show evidence of PAHs on their surfaces. The fact that they all contain large amounts of m/z 206 and 220 show that the origin of the PAHs is primarily hydrogenated fuel combustion (i.e., diesel combustion). In Kittleson's review of engines and nanoparticles (*31*), he noted that diesel soot particles are aggregates of nanoparticles (2−50 nm) and condensates from the exhaust gases. When these particles come into physical contact with other particles, nanoparticles from the soot aggregate can be transferred to the surface of the other particle. The amount of material that is transferred depends on how strongly the other particle adsorbs it and how tightly it is bound to the soot aggregate. The particles that co-desorb potassium and calcium probably are soil- or ash-derived. These particles are known to adsorb PAHs strongly (*27*), so it is not surprising to find large amounts of PAHs on these particle surfaces. We noted that PAHs were associated with the majority of the particles that yielded significant signal. Many of the sampled particles showed sharp PAH mass lines with low intensity. The origin of this type of surface component is not completely clear. They may be the result of weak physical interactions between the particles in the collected sample. Alternatively, they could arise from vapor deposition because the particle-bound PAHs have a finite vapor pressure and the sample was stored for many years. However, in this case, one would expect the PAH distribution to be skewed because vapor pressure decreases with increasing PAH size. More work is needed to resolve these issues.

The above results suggest that the final fate of the PAHs derived from diesel soot particles is to be smeared across every available surface until they eventually degrade. Moreover, they demonstrate that material transfer may occur when particles come in to physical contact with each other and surfaces. This process could profoundly affect the chemistry in the atmosphere and human health. The role of particles in material transfer has yet to be investigated; however, we now have the means.

Acknowledgments

This research was sponsored by the Office of Research and Development, U.S. Department of Energy, under Contract DE-AC05-96OR22464 with Oak Ridge National Laboratory managed by Lockheed Martin Energy Research Corp.

Literature Cited

(1) Sinha, M. P. *Rev. Sci. Instrum*. **1984**, *55*, 886.
(2) McKeown, P. J.; Johnston, M. V.; Murphy, D. M. *Anal. Chem*. **1991**, *63*, 2069.
(3) Kievit, O.; Marijinissen, J. C. M.; Verheijen, P. J. T.; Scarlett, B. *J. Aerosol Sci.* **1992**, *23* (Suppl. 1), S301.
(4) Prather, K. A.; Nordmeyer, T.; Salt, K. *Anal. Chem*. **1994**, *66*, 1403.
(5) Hinz, K. P.; Kaufmann, R.; Spengler, B. *Anal. Chem*. **1994**, *66*, 2071.
(6) Murphy, D. M.; Thomson, D. S. *Aerosol Sci. Technol.* **1995**, *22*, 237.
(7) Carson, P. G.; Neubauer, K. R.; Johnston, M. V.; Wexler, A. S. *J. Aerosol Sci*. **1995**, *26*, 535.
(8) Reents, W. D., Jr.; Downey, S. W.; Emerson, A. B.; Mujsce, A. M.; Miller, A. J.; Siconolfi, D. J.; Sinclair, J. D.; Swanson, A. G. *Aerosol Sci. Technol.* **1995**, *23*, 263.
(9) Reilly, P. T. A.; Gieray, R. A.; Yang, M.; Whitten, W. B.; Ramsey, J. M. *Anal. Chem*. **1997**, *69*, 36.
(10) Gieray, R. A.; Reilly, P. T. A.; Yang, M.; Whitten, W. B.; Ramsey, J. M. *J. Microbiol. Methods* **1997**, *29*, 191.
(11) Yang, M.; Reilly, P. T. A.; Borass, K. B.; Whitten, W. B.; Ramsey, J. M. *Rapid Commun. Mass Spectrom*. **1996**, *10*, 347.
(12) Reilly, P. T. A.; Lazar, A. C.; Whitten, W. B.; Ramsey, J. M. *Aerosol Sci. Technol.* In press.
(13) Morrical, B. D.; Fergenson, D. P.; Prather, K. A. *J. Am. Soc. Mass Spectrom*. **1998**, *9*, *10*, 1068.
(14) Clemett, S. J.; Maechling, C. R.; Zare, R. N.; Swan, P. D.; Walker, R. M. *Science* **1993**, *262*, 721.
(15) Dale, M. J.; Jones, A. C.; Pollard, S. J. T.; Langridge-Smith, P. R. R.; Rowely, A. G. *Environ. Sci. Technol.* **1993**, *27*, 1693.
(16) Zhan, Q.; Voumard, P.; Zenobi, Z. *Rapid Commun. Mass Spectrom*. **1995**, *9*, 119.
(17) Hankin, S. M.; John, P.; Simpson, A. W.; Smith, G. P. *Anal. Chem*. **1996**, *68*, 3238.
(18) Kornienko, O.; Ada, E. T.; Tinka, J.; Wijesundara, M. B. J.; Hanley, L. *Anal. Chem*. **1998**, *70*, 1208.
(19) Reilly, P. T. A.; Gieray, R. A.; Yang, M.; Whitten, W. B.; Ramsey, J. M. *Anal. Chem*. **1997**, *69*, 36.
(20) Gieray, R. A.; Reilly, P. T. A.; Yang, M.; Whitten, W. B.; Ramsey, J. M. *J. Microbiol. Methods* **1997**, *29*, 191.
(21) Gieray, R. A.; Reilly, P. T. A.; Yang, M.; Whitten, W. B.; Ramsey, J. M. *Anal. Chem*. **1998**, *70*, 117.
(22) Reilly, P. T. A.; Gieray, R. A.; Whitten, W. B.; Ramsey, J. M. Manuscript in preparation.
(23) Nourse, B. D.; Cox, K. A.; Morand, K. L.; Cooks, R. G. *J. Am. Chem. Soc.* **1992**, *114*, 2010.
(24) http://webbook.nist.gov.
(25) Reilly, P. T. A.; Gieray, R. A.; Whitten, W. B.; Ramsey, J. M. *Environ. Sci. Technol.* **1998**, *32*, 2672.
(26) Gray, H. A.; Cass, G. R. *Atmos. Environ*. **1998**, *32*, 3805.
(27) Gillette, J. S.; Luthy, R. G.; Clemett, S. J.; Zare, R. N. *Environ. Sci. Technol.* **1999**, *33*, 1185.
(28) Reilly, P. T. A.; Gieray, R. A.; Whitten, W. B.; Ramsey, J. M. *Combust. Flame*, submitted for publication.
(29) Hankin, S. M.; John, P. *Anal. Chem*. **1999**, *71*, 1100.
(30) A 64% miss rate for the two-laser experiment as compared with the typical 33% miss rate for the one-laser experiment is not surprising given the jitter in the timing, the overlap of the two focal points, and the delay between the lasers. Similar results were observed by Morrical et al. (*13*).
(31) Kittelson, D. B. *J. Aerosol Sci.* **1998**, *29*, 575.

Received for review May 24, 1999. Revised manuscript received August 9, 1999. Accepted September 7, 1999.

ES9905849